THE JOURNAL OF BIOLOGICAL CHEMISTRY VOL. 281, NO. 18, pp. 12315–12324, May 5, 2006

Kinetic Evidence for Inefficient and Error-prone Bypass across Bulky N^2-Guanine DNA Adducts by Human DNA Polymerase ι*[S]

Received for publication, January 5, 2006, and in revised form, February 6, 2006 Published, JBC Papers in Press, March 8, 2006, DOI 10.1074/jbc.M600112200

Jeong-Yun Choi[1] **and F. Peter Guengerich**[2]

From the Department of Biochemistry and Center in Molecular Toxicology, Vanderbilt University School of Medicine, Nashville, Tennessee 37232-0146

DNA polymerase (pol) ι has been proposed to be involved in translesion synthesis past minor groove DNA adducts via Hoogsteen base pairing. The N2 position of G, located in minor groove side of duplex DNA, is a major site for DNA modification by various carcinogens. Oligonucleotides with varying adduct size at G N2 were analyzed for bypass ability and fidelity with human pol ι. Pol ι effectively bypassed N^2-methyl (Me)G and N^2-ethyl(Et)G, partially bypassed N^2-isobutyl(Ib)G and N^2-benzylG, and was blocked at N^2-CH_2(2-naphthyl)G (N^2-NaphG), N^2-CH_2(9-anthracenyl)G (N^2-AnthG), and N^2-CH_2(6-benzo[*a*]pyrenyl)G. Steady-state kinetic analysis showed decreases of k_{cat}/K_m for dCTP insertion opposite N^2-G adducts according to size, with a maximal decrease opposite N^2-AnthG (61-fold). dTTP misinsertion frequency opposite template G was increased 3–11-fold opposite adducts (highest with N^2-NaphG), indicating the additive effect of bulk (or possibly hydrophobicity) on T misincorporation. N^2-IbG, N^2-NaphG, and N^2-AnthG also decreased the pre-steady-state kinetic burst rate compared with unmodified G. High kinetic thio effects (S_p-2′-deoxycytidine 5′-*O*-(1-thiotriphosphate)) opposite N^2-EtG and N^2-AnthG (but not G) suggest that the chemistry step is largely interfered with by adducts. Severe inhibition of polymerization opposite N^2,N^2-diMeG compared with N^2-EtG by pol η but not by pol ι is consistent with Hoogsteen base pairing by pol ι. Thus, polymerization by pol ι is severely inhibited by a bulky group at G N2 despite an advantageous mode of Hoogsteen base pairing; pol ι may play a limited role in translesion synthesis on bulky N^2-G adducts in cells.

The accurate and efficient replication of DNA is crucial for preservation of genomic integrity and survival of organisms (1). The major obstacle for DNA replication is various DNA lesions that are inevitably formed by both endogenous sources and exogenous mutagens in cells, some of which escape repair and are usually present in replicating DNA (2). When encountering lesions during DNA replication, DNA polymerases often show abnormal behavior, misinsertion of incorrect nucleotides, slippage, and blockage of replication, which cause mutation or cell death, leading in turn to detrimental effects, including aging and cancer (3). Replicative DNA polymerases, which have high fidelity and efficiency with unmodified DNA bases, are intolerant of the geometric DNA distortions caused by many DNA lesions and thus are blocked (and/or misinsert bases inefficiently) opposite modified DNA adducts during replication. To cope with this replication barrier, organisms utilize TLS[2] DNA polymerases, which have more open and larger active sites and can synthesize DNA across and beyond various replication-blocking DNA lesions (4, 5). Most eukaryotic TLS DNA polymerases belong to the recently discovered Y-family, including pol η, pol ι, pol κ, and Rev1 (3, 6). Although TLS DNA polymerases can readily accommodate and replicate through bulkier DNA lesions than replicative DNA polymerases, their synthesis can still be inhibited (or blocked) by certain DNA lesions, and bypass can be error-prone or error-free, depending on the adduct (7).

The N2 atom of guanine is susceptible to modification by various potential carcinogens, including formaldehyde (8), acetaldehyde (9) (a metabolite of ethanol and also produced endogenously), styrene oxide (10), oxidation products of heterocyclic aromatic amines (*e.g. N*-hydroxy-2-amino-3-methylimidazo[4,5-*f*]quinoline and *N*-hydroxy-2-amino-3,8-dimethylimidazo[4,5-*f*]quinoxaline (11, 12)), and the oxidation products of various polycyclic aromatic hydrocarbons (*e.g.* benzo[*a*]pyrene (13, 14)). N^2-ethyl deoxyguanosine has been detected in granulocyte and lymphocyte DNA and urine of alcoholic patients (15, 16). Even the relatively small N^2-MeG and N^2-EtG adducts have been reported to be miscoding with Klenow fragment (*Escherichia coli* DNA polymerase I) and its exonuclease$^-$ form, pol T7$^-$, and HIV-1 RT (8, 9, 17). N^2-EtG and larger N^2-G adducts cause the strong blockage of polymerization by pol T7$^-$ and HIV-1 RT (17) but are bypassed efficiently and accurately by human pol η, but with some limitation by adduct size (18).

Pol ι has distinctive enzymatic properties in replicating four template bases with very different efficiencies and fidelities (19–21). Pol ι exhibits higher efficiencies of polymerization opposite purines (A and G; A being greater) than pyrimidines (C and T), and lower fidelities opposite T (lowest) and G than opposite A and C. Although pol ι can incorporate nucleotides opposite certain DNA lesions, such as an abasic site, the 3′ T of (6–4)-T-T photoproducts, a benzo[*a*]pyrene adduct of dA, and 8-hydroxy-1,N^2-propanoG *in vitro* (20, 22–24), the biological role of pol ι in TLS remains largely unknown. Pol ι has been proposed to bypass bulky minor groove purine lesions, such as N^2-G adducts due to a unique Hoogsteen base-pairing mode opposite template purines in the active site (25, 26). However, detailed kinetic evidence to support this

* This work was supported in part by United States Public Health Service Grants R01 ES10375 and P30 ES00267 (to F. P. G.). The costs of publication of this article were defrayed in part by the payment of page charges. This article must therefore be hereby marked "*advertisement*" in accordance with 18 U.S.C. Section 1734 solely to indicate this fact.

[S] The on-line version of this article (available at http://www.jbc.org) contains a MALDI-TOF mass spectrum and capillary gel electrophoretogram of the synthetic oligonucleotide containing N^2,N^2-diMeG and SDS-polyacrylamide gel electrophoretic analysis of purified DNA polymerase ι.

[1] Present address: Dept. of Pharmacology, College of Medicine, Ewha Womans University, 911-1 Mok-6-Dong, Yangcheon-Gu, Seoul, 158-710, Republic of Korea.

[2] To whom correspondence should be addressed: Dept. of Biochemistry and Center in Molecular Toxicology, Vanderbilt University School of Medicine, 638 Robinson Research Bldg., 23rd and Pierce Aves., Nashville, TN 37232-0146. Tel.: 615-322-2261; Fax: 615-322-3141; E-mail: f.guengerich@vanderbilt.edu.

[2] The abbreviations used are: TLS, translesion synthesis; Et, ethyl; Ib, isobutyl; Bz, benzyl; N^2-Naph, N^2-methyl(2-naphthyl); N^2-Anth, N^2-methyl(9-anthracenyl); N^2-BP, N^2-methyl(6-benzo[*a*]pyrenyl); BPDE, benzo[*a*]pyrene diol epoxide; dCTPαS, 2′-deoxycytidine 5′-*O*-(1-thiotriphosphate); MALDI-TOF, matrix-assisted laser desorption ionization time-of-flight; 8-oxoG, 8-oxo-7,8-dihydroG; pol, DNA polymerase; RT, reverse transcriptase.

view has not yet been presented. Recent reports suggest a possible role of pol ι in carcinogenesis. For instance, the pol ι gene has been shown to be a modifier of mouse lung tumorigenesis (27). Pol ι is overexpressed in certain types of human cancer samples and breast cancer cells, which may lead to reduction of DNA replication fidelity (28, 29).

The molecular size of DNA adducts, along with shape and chemical properties, may be a key differentiating factor in the blockage and misincorporation of DNA polymerases, which have confined active site pockets. The bulkiness of DNA adducts is important in understanding mechanisms of mutagenesis, especially caused by environmental chemicals (30). We have previously studied some of the details of blockage and misincorporation with the model replicative DNA polymerases pol T7$^-$ and HIV-1 RT in work focused on various modifications of G at the C8 (8-oxoG), O6 (O^6-MeG and O^6-BzG), and N2 atoms (N^2-MeG, N^2-EtG, N^2-IbG, N^2-BzG, N^2-AnthG, N^2-(2,3,4-trihydroxy-1-butyl)G, 8-hydroxy-1,N^2-propanoG, 8-hydroxy-6-methyl-1,N^2-propanoG, and the styrene oxide and BPDE products formed at the G N2 atom) of guanine (17, 31–35). Small adducts, such as 8-oxoG, O^6-MeG, and N^2-MeG, are bypassed fairly readily with some misincorporations, depending upon the polymerase (32, 33, 36). However, with other bulky adducts, the polymerase catalytic efficiency and fidelity are dramatically decreased. The effect of adduct size is consistently seen in one TLS polymerase, pol η, although pol η is more resistant to bulky adducts than pol T7$^-$ and HIV-1 RT (18). In the present work, we systematically evaluated the effect of varying size at the guanine N2 atom in studying human pol ι, which has been proposed to bypass bulky N^2-G adducts via a Hoogsteen base-pairing mode. We prepared site-specifically modified oligonucleotides containing N^2-MeG, N^2-EtG, N^2,N^2-diMeG, N^2-IbG, N^2-BzG, N^2-NaphG, N^2-AnthG, and N^2-BPG adducts (*i.e.* with gradually increasing size at the guanine N^2-adduct) (Fig. 1) and used these with pol ι. Steady-state and pre-steady-state kinetics were investigated, along with the features of DNA substrate and dNTP binding to pol ι. DNA polymerization by human pol ι is moderately tolerated up to the size of N^2-BzG but strongly interfered with by bulk equal to or larger than N^2-NaphG, in a size-dependent manner. The hydrophobicity increases along with bulk and may also be a contributing factor. The mechanism of interference is discussed in the context of the kinetic behavior of pol ι with bulky N^2-G adducts.

EXPERIMENTAL PROCEDURES

Materials—Unlabeled dNTPs were purchased from Amersham Biosciences. S_p-dCTPαS and R_p-dCTPαS were purchased from Biolog Life Science Institute (Bremen, Germany). [γ-^{32}P]ATP (specific activity 3,000 Ci/mmol) was purchased from PerkinElmer Life Sciences. T4 polynucleotide kinase and restriction endonucleases were purchased from New England Biolabs (Beverly, MA). Bio-spin columns were purchased from Bio-Rad. Protease inhibitor mixture was obtained from Roche Applied Science. Human testis cDNA was purchased from BD Biosciences Clontech (Palo Alto, CA). *Pfu ultra* DNA polymerase and pPCR-Script Amp vector were purchased from Stratagene (La Jolla, CA). BaculoGold transfection kits were obtained from BD Biosciences Pharmingen (San Diego, CA). Amicon Ultra centrifugal filter devices were purchased from Millipore Corp. (Billerica, MA).

Oligonucleotides—The unmodified 24-mer, 25-mers, and 36-mer (Table 1) were purchased from Midland Certified Reagent Co. (Midland, TX). Seven 36-mers, each containing a guanine N^2-adduct (*e.g.* N^2-MeG, N^2-EtG, N^2-IbG, N^2-BzG, N^2-NaphG, N^2-AnthG, and N^2-BPG), were prepared as previously described (17, 18). The 36-mer containing an N^2,N^2-diMeG was prepared according to a postoligomerization methodology (37) using a 2-fluoro-O^6-(trimethylsilylethyl)-2′-deoxyinosine-containing 36-mer and dimethylamine and purified by high pressure liquid chromatography and denaturing polyacrylamide gel electrophoresis (17). MALDI-TOF mass spectrometry and capillary gel electrophoresis were used to confirm the correct M_r value and purity for the oligonucleotide (see supplemental data). The extinction coefficients for the oligonucleotides, estimated by the Borer method (38), were as follows: 24-mer, ϵ_{260} = 224 mM^{-1} cm^{-1}; 25-mer, ϵ_{260} = 232 mM^{-1} cm^{-1}; 36-mer, ϵ_{260} = 310 mM^{-1} cm^{-1}.

TABLE 1
Oligodeoxynucleotides used in this study

Oligodeoxynucleotide	Sequence
24-mer	5′-GCCTCGAGCCAGCCGCAGACGCAG
25C-mer	5′-GCCTCGAGCCAGCCGCAGACGCAGC
25T-mer	5′-GCCTCGAGCCAGCCGCAGACGCAGT
36-mer	3′-CGGAGCTCGGTCGGCGTCTGCGTCG*CT-CCTGCGGCT[a]

[a] G*, G, N^2-MeG, N^2-EtG, N^2-IbG, N^2-BzG, N^2-NaphG, N^2-AnthG, N^2-BPG, or N^2, N^2-diMeG.

Isolation of Human POLI cDNA and Construction of Recombinant Baculovirus—Human DNA polymerase ι cDNA was obtained by PCR amplification from human testis cDNA (as template) using *Pfu ultra* DNA polymerase with the corresponding two primers 5′-CTCGAGGCATGGAACTGGCGGACGT-3′ and 5′-TCCCTTGCTTTTCAGACCTT-3′. The resulting 2.2-kb PCR product of *POLI* was cloned into the vector pPCR-Script Amp, and nucleotide sequencing was done to confirm the entire sequence of the coding region. The fragment containing the human *POLI* gene was cloned into the XhoI and NotI sites of the vector pAcHLT-B to generate a fusion tag containing six histidines at the N terminus, yielding the vector pAcHLT/HPOLI. This plasmid was co-transfected into Sf9 insect cells with BaculoGold DNA using a BaculoGold transfection kit to generate the recombinant baculovirus expressing human pol ι.

Expression and Purification of Human DNA Polymerases—Recombinant human pol ι was expressed in Sf9 insect cells (2×10^9 cells) with the amplified recombinant baculovirus for 60 h. The harvested cell pellets were lysed in 100 ml of Buffer A (50 mM Tris-HCl (pH 7.5) containing 500 mM NaCl, 10% glycerol (v/v), 5 mM β-mercaptoethanol, 0.5% (v/v) Nonidet P-40, and protease inhibitor mixture). The cell debris was removed by ultracentrifugation at $10^5\times$ *g* for 60 min. The resulting supernatant was loaded onto a 5-ml HisTrap column (Amersham Biosciences) and washed sequentially with 50 ml of buffer B (50 mM Tris-HCl (pH 7.5) containing 500 mM NaCl, 10% glycerol (v/v), and 5 mM β-mercaptoethanol) containing 20 mM imidazole and then with 50 ml of Buffer B containing 40 mM imidazole and finally with 50 ml of Buffer B containing 50 mM imidazole. Bound proteins were eluted with 400 mM imidazole in Buffer B. Eluted proteins were dialyzed against Buffer C (50 mM Tris-HCl (pH 7.5) containing 10% (v/v) glycerol and 5 mM β-mercaptoethanol) and loaded onto a 1-ml MonoQ column (Amersham Biosciences). Pol ι was eluted with a 30-ml linear gradient of 0–1.0 M NaCl in Buffer C. Eluted fractions were analyzed by SDS-polyacrylamide gel electrophoresis, with silver staining (39), and pol ι was found to be eluted at 100 mM NaCl. Pooled pol ι fractions were concentrated using an Amicon Ultra centrifugal filter device to a volume of 100 μl and were further purified to near homogeneity using a Superdex 200 column (Amersham Biosciences) with Buffer C containing 150 mM NaCl (see supplemental data). The active enzyme concentration of pol ι was determined by the active site titration method described below. Recombinant human pol η was prepared as described previously (18).

Reaction Conditions for Enzyme Assays—Unless indicated otherwise, standard DNA polymerase reactions were performed in 50 mM Tris-HCl (pH 7.5) buffer containing 5 mM dithiothreitol, 100 μg of bovine

serum albumin/ml (w/v), and 10% glycerol (v/v) with 100 nM primer-template at 37 °C. Primers were 5′-end-labeled using T4 polynucleotide kinase with [γ-^{32}P]ATP and annealed with template (36-mer). All reactions were initiated by the addition of dNTP and $MgCl_2$ (5 mM final concentration) to preincubated enzyme/DNA mixtures.

Primer Extension Assay with All Four dNTPs—A ^{32}P-labeled primer, annealed to either an unmodified or adducted template, was extended in the presence of all four dNTPs (100 μM each) for 15 min. Reaction mixtures (8 μl) were quenched with 2 volumes of a solution of 20 mM EDTA in 95% formamide (v/v). Products were resolved using a 16% polyacrylamide (w/v) gel electrophoresis system containing 8 M urea and visualized with a Bio-Rad Molecular Imager FX and Quantity One software (Bio-Rad).

Steady-state Reactions—A ^{32}P-labeled primer, annealed to either an unmodified or adducted template, was extended in the presence of increasing concentrations of a single dNTP. The molar ratio of primer-template to enzyme was at least 10:1. Enzyme concentrations and reaction times were chosen so that maximal product formation would be ≤20% of the substrate concentration (40). The primer-template was extended with dNTP in the presence of 0.1–5 nM enzyme for 5 or 10 min. All reactions (8 μl) were done at 10 dNTP concentrations (in duplicate) and quenched with 2 volumes of a solution of 20 mM EDTA in 95% formamide (v/v). Products were resolved using a 16% polyacrylamide (w/v) electrophoresis gel containing 8 M urea and quantitated by phosphorimaging analysis using a Bio-Rad Molecular Imager FX instrument and Quantity One software. Graphs of product formation *versus* dNTP concentration were fit using nonlinear regression (hyperbolic fits) in GraphPad Prism version 3.0 (San Diego, CA) for the determination of k_{cat} and K_m values.

Pre-steady-state Reactions—Rapid quench experiments were performed using a model RQF-3 KinTek Quench Flow Apparatus (KinTek Corp., Austin, TX). Reactions were initiated by rapid mixing of ^{32}P-primer-template/polymerase mixtures (12.5 μl) with the dNTP-Mg^{2+} complex (10.9 μl) and then quenched with 0.3 M EDTA after times varying from 5 ms to 4 s (or 30 s for N^2-IbG-, N^2-NaphG-, and N^2-AnthG-containing oligonucleotides). Reactions were mixed with 450 μl of formamide-dye solution (20 mM EDTA, 95% formamide (v/v), 0.5% bromphenol blue (w/v), and 0.05% xylene cyanol (w/v)) and run on a denaturing electrophoresis gel, with quantitation as described for the steady-state reactions. Pre-steady-state experiments were fit with the burst equation $y = A(1 - e^{-kpt}) + k_{ss}t$, where y represents the concentration of product, A is burst amplitude, k_p is pre-steady-state rate of nucleotide incorporation, t is time, and k_{ss} is the steady-state rate of nucleotide incorporation (not normalized for enzyme concentration in the equation) (41, 42), using nonlinear regression analysis in GraphPad Prism version 3.0.

Phosphorothioate Analysis—With the ^{32}P-primer annealed to either an unmodified or adducted template, reactions were initiated by rapid mixing of ^{32}P-primer-template/polymerase mixtures (12.5 μl) with S_p-dCTPαS-Mg^{2+} complex (or dCTP-Mg^{2+}) (10.9 μl) and then quenched with 0.3 M EDTA after reaction times varying from 5 ms to 4 s (or 30 s for N^2-AnthG-containing DNA). Products were analyzed as described for the pre-steady-state reactions mentioned earlier.

DNA Dissociation from Pol ι k_{off} Measurements—DNA dissociation rates from the polymerase-oligonucleotide complex (*E*·DNA) were determined using a rapid quench-flow apparatus (33, 43, 44). Preincubated solutions of pol ι (350 nM) and unlabeled target DNA (24-mer/36-mer; 50 nM) were rapidly mixed with ^{32}P-labeled 24-mer/36-G-mer (450 nM) for times of 0.8–4 s, and then polymerization was initiated by the addition of 1 mM dNTP-Mg^{2+} from the central drive syringe, for a

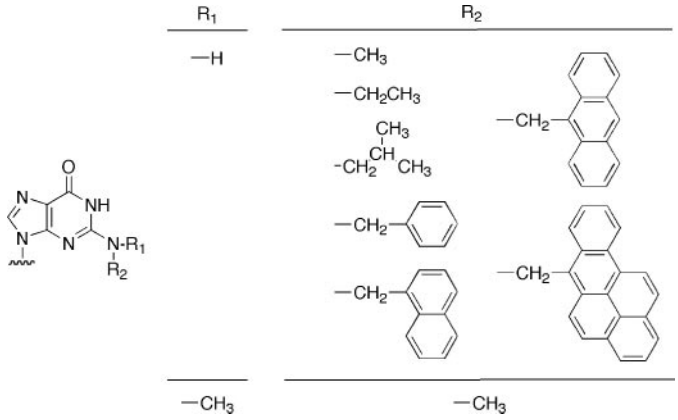

FIGURE 1. ***N^2*-Guanine derivatives used in this work.**

constant reaction time of 0.5 s. Expelled samples from the apparatus were rapidly mixed into tubes containing 500 μl of 0.3 M EDTA (in 50% formamide (v/v)) to stop the reaction. Products were quantified by gel electrophoretic analysis. Graphs of nM product *versus* time were fit using the equation, $y = E_f + E_0(1 - e^{-kt})$, where y represents the concentration of product, E_f is the free enzyme concentration, E_0 is the DNA-bound enzyme concentration, k_{off} is the dissociation rate of DNA from *E*·DNA, and t is time (33, 45), using nonlinear regression in GraphPad Prism version 3.0.

Active Site Titration and Determination of K_d^{DNA}—The K_d^{DNA} for productive binding of pol ι to 24-mer/36-mer DNA substrates was determined using pre-steady-state analysis. Pol ι, preincubated with increasing concentrations of the DNA substrate in sample syringe A, was mixed with saturating dCTP-Mg^{2+} from sample syringe B and then quenched with 0.3 M EDTA after times of 0.5 s. A graph of the burst amplitude *versus* total DNA concentration was plotted and fit to a quadratic equation, $A = 0.5(K_d + E_t + D_t) - [(0.25(K_d + E_t + D_t)^2 - E_tD_t)]^{1/2}$, where A represents burst amplitude, E_t is the active enzyme concentration, D_t is DNA concentration, and K_d is the equilibrium dissociation constant for productive DNA binding (41, 42) in GraphPad Prism version 3.0.

Determination of K_d^{dCTP}—K_d^{DNA} was estimated by performing pre-steady-state reactions at different dNTP concentrations with reaction times varying from 5 ms to 4 s. A graph of the burst rate (k_{obs}) *versus* dCTP concentration was fit to the hyperbolic equation, $k_{obs} = k_{pol}[dNTP]/([dNTP] + K_d)$, where k_{pol} represents the maximal rate of nucleotide incorporation and K_d^{dCTP} is the equilibrium dissociation constant for dCTP (41, 42).

RESULTS

Primer Extension by Human Pol ι in the Presence of All Four dNTPs—Processive polymerization by human pol ι at various N^2-G adducts, in the presence of all four dNTPs, was analyzed in "standing start" assays using 24-mer/36-mer duplexes containing G and each of seven different N^2-G adducts (Fig. 1) at position 25 of the template (Fig. 2). Pol ι readily extended the 24-mer primer annealed to the unmodified G, N^2-MeG, and N^2-EtG templates in proportion to the concentration of enzyme, mainly up to 27- and 28-mer products (with some 25-, 26-, 29-, 30-, and 31-mer products) but yielded no full-length 36-mer products. Polymerization with N^2-IbG and N^2-BzG derivatives yielded a pattern of extension similar to unmodified G but partially blocked in the steps of incorporation opposite the lesion (N^2-IbG and N^2-BzG) and/or the subsequent extension (N^2-BzG). The polymerization of N^2-NaphG, N^2-AnthG, and N^2-BPG yielded only 1-base extension products, indi-

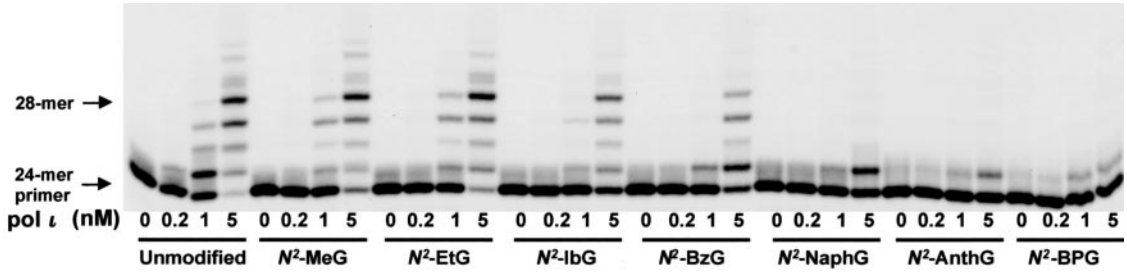

FIGURE 2. **Extension of ^{32}P-labeled primers opposite G, N^2-MeG, N^2-EtG, N^2-IbG, N^2-BzG, N^2-NaphG, N^2-AnthG, and N^2-BPG by human pol ι in the presence of all four dNTPs.** Primer (24-mer) was annealed with each of the eight different 36-mer templates (Table 1) containing an unmodified G or N^2-modified G placed at the 25th position from the 3′-end. Reactions were done for 15 min with increasing concentrations of pol ι (0–5 nM) and a constant concentration of DNA substrate (100 nM primer-template) as indicated. ^{32}P-labeled 24-mer primer was extended in the presence of all four dNTPs. The reaction products were analyzed by denaturing gel electrophoresis with subsequent phosphorimaging analysis.

TABLE 2
Steady-state kinetic parameters for one-base incorporation by human pol ι

Template	dNTP	K_m	k_{cat}	k_{cat}/K_m	f (misinsertion ratio)
		μM	s^{-1}	$mM^{-1}\,s^{-1}$	
G	C	88 ± 12	0.23 ± 0.01	2.6	1
	T	640 ± 60	0.30 ± 0.01	0.47	0.18
N^2-MeG	C	330 ± 20	0.091 ± 0.002	0.28	1
	T	1600 ± 200	0.22 ± 0.01	0.14	0.50
N^2-EtG	C	190 ± 30	0.12 ± 0.01	0.63	1
	T	1100 ± 100	0.38 ± 0.01	0.35	0.56
N^2-IbG	C	320 ± 60	0.066 ± 0.004	0.21	1
	T	1100 ± 100	0.15 ± 0.01	0.14	0.67
N^2-BzG	C	770 ± 160	0.075 ± 0.007	0.10	1
	T	1100 ± 150	0.20 ± 0.01	0.18	1.8
N^2-NaphG	C	370 ± 50	0.040 ± 0.002	0.11	1
	T	1300 ± 160	0.19 ± 0.01	0.15	1.36
N^2-AnthG	C	260 ± 30	0.011 ± 0.001	0.042	1
	T	340 ± 40	0.014 ± 0.001	0.041	0.98
N^2-BPG	C	76 ± 12	0.0093 ± 0.0001	0.12	1
	T	120 ± 20	0.012 ± 0.001	0.10	0.83

cating that pol ι was strongly blocked at the site of those lesions and the subsequent extension step. Even a much higher concentration (50 nM instead of 5 nM) of pol ι could generate only 1-base extension products with those lesions (results not shown). Thus, there were gradual attenuations of the ability of pol ι with increasing size of adducts in two steps: (i) incorporation opposite the lesion (N^2-IbG and larger adducts) and (ii) subsequent extension (N^2-BzG and larger adducts).

Steady-state Kinetics of dNTP Incorporation Opposite G and N^2-G Adducts—Steady-state parameters were measured for dNTP incorporation into 24-mer/36-mer duplexes opposite G and N^2-G adducts (Table 2). The incorporations of dATP and dGTP opposite G and N^2-G adducts by pol ι were not determined because of much less efficient activity than with other dNTPs. Pol ι preferentially incorporated dCTP opposite G but with high misinsertion frequency, $f = (k_{cat}/K_m)_{dNTP}/(k_{cat}/K_m)_{dCTP}$ (where dNTP ≠ dCTP) for dTTP (f = 0.2). All N^2-G adducts further increased the misinsertion frequencies by 3–11-fold. The increase in the misinsertion frequency of T was attributable more to the larger decrease of k_{cat}/K_m for correct dCTP insertion than that of the more favorable dTTP insertion.

For the correct incorporation of dCTP, the catalytic efficiency (k_{cat}/K_m) was decreased (9-fold) opposite N^2-MeG compared with unmodified G. The catalytic efficiency of dCTP incorporation was further decreased with increasing size of adducts, although changes in k_{cat}/K_m opposite N^2-EtG and N^2-BPG were not in order. The largest decrease (61-fold) of k_{cat}/K_m, opposite N^2-AnthG, was due to both the decrease of k_{cat} and the increase of K_m. For incorrect dTTP incorporation, k_{cat}/K_m decreased opposite various N^2-G adducts, similar to dCTP but to a lesser extent than for dCTP.

Steady-state Kinetics of Next-base Extension following dCTP or dTTP Insertion Opposite G and N^2-G Adducts—Steady-state kinetic analysis of next-base extension (Table 3) was performed to analyze the effect of bulk at guanine N2 on next-base extension ability from the correct base pair, G (or N^2-G adducts):C or the mispair, G (or N^2-G adducts):T by pol ι. Pol ι extended the correct base pair much more effectively than the mispair. The k_{cat}/K_m for incorporation of the correct next nucleotide (dGTP) following the correct base G:C pair did change variably, irrespective of the size of adducts. Beyond N^2-MeG:C and N^2-EtG:C base pairs, k_{cat}/K_m for dGTP incorporation was increased 3- and 9-fold, compared with the G:C base pair. Thereafter, the k_{cat}/K_m for next-base extension from N^2-BzG:C or N^2-NaphG:C base pairs was decreased (8–170-fold) gradually, compared with an N^2-G:C base pair. The k_{cat}/K_m for dGTP incorporation from the G (or G-adducts):T mispairs changed in a pattern similar to the "matched" G (G-adducts):C pairs and was much lower (10–200-fold) than from matched pairs with C. Overall, the "misextension ratio" (f_{ext}), where $f_{ext} = (k_{cat}/K_m)_{mispair}/(k_{cat}/K_m)_{correct\ pair}$ (40, 46), was variable but relatively low (0.005–0.1) and highest with the adducts N^2-MeG and N^2-NaphG.

Pre-steady-state Burst Kinetics of dCTP Incorporation Opposite G, N^2-EtG, N^2-IbG, and N^2-AnthG by Pol ι—In order to characterize the kinetics within the catalytic cycle of pol η, pre-steady-state reactions were performed in a rapid quench-flow instrument using oligonucleotide concentrations 4-fold greater than the enzyme concentration. Preformed *E*·DNA complexes were mixed with saturating concentrations of dCTP-Mg^{2+} and then quenched following varying reaction times (Fig. 3). Pol ι clearly showed biphasic kinetics for correct dCTP incorporation opposite G. The first phase of the cycle (*i.e.* the burst phase) was finished in ~500 ms with oligonucleotides containing G and N^2-EtG. For the oligonucleotides containing N^2-IbG, N^2-NaphG, and N^2-AnthG, the burst was marginally detectable in ~2 s (N^2-IbG and N^2-NaphG) and ~8 s (N^2-AnthG). Pol ι incorporation of dCTP into the 24-mer/36-G-mer occurred with a burst rate of k_p = 3.6 ± 0.5 s^{-1} (Fig. 3). The (burst) rate decreased proportionally with increasing bulk.

TABLE 3
Steady-state kinetic parameters for next-base extension from G (or N^2-G adduct):C (or T) template-primer termini by human pol ι

Base pair at 3′ primer termini (template-primer)	Extension with dGTP (the next correct nucleotide against template C)			
	K_m	k_{cat}	k_{cat}/K_m	f_{ext} (misextension efficiency)
	μM	s^{-1}	$mM^{-1}\ s^{-1}$	
G:C	150 ± 10	0.26 ± 0.01	1.7	1
G:T	520 ± 50	0.025 ± 0.001	0.048	0.028
N^2-MeG:C	65 ± 7	0.32 ± 0.01	4.9	1
N^2-MeG:T	220 ± 20	0.099 ± 0.003	0.45	0.092
N^2-EtG:C	37 ± 3	0.56 ± 0.01	15	1
N^2-EtG:T	97 ± 12	0.039 ± 0.001	0.40	0.027
N^2-IbG:C	95 ± 12	0.24 ± 0.01	2.5	1
N^2-IbG:T	200 ± 20	0.0078 ± 0.0003	0.039	0.016
N^2-BzG:C	300 ± 50	0.063 ± 0.004	0.21	1
N^2-BzG:T	230 ± 40	0.0011 ± 0.0001	0.0047	0.022
N^2-NaphG:C	400 ± 80	0.0042 ± 0.0001	0.01	1
N^2-NaphG:T	220 ± 50	0.00037 ± 0.00002	0.0016	0.16
N^2-AnthG:C	42 ± 2	0.038 ± 0.001	0.90	1
N^2-AnthG:T	120 ± 30	0.00066 ± 0.00003	0.0055	0.006
N^2-BPG:C	51 ± 5	0.018 ± 0.001	0.35	1
N^2-BPG:T	300 ± 70	0.0015 ± 0.0001	0.005	0.014

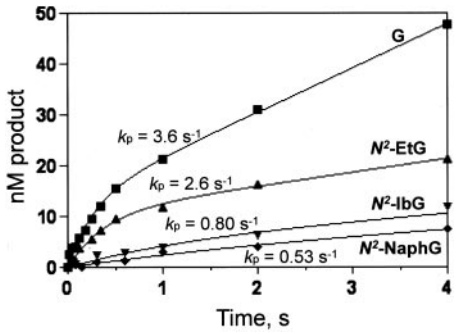

FIGURE 3. **Pre-steady-state burst kinetics of incorporation opposite G, N^2-EtG, N^2-IbG, and N^2-NaphG by human pol ι.** Pol ι (24 nM) was incubated with 100 nM 24-mer/36-mer primer-template complex in a rapid quench-flow instrument and mixed with dCTP (and $MgCl_2$) to initiate reactions: 1 mM dCTP for the 24-mer/36-G-mer (■), 24-mer/36-N^2-EtG-mer (▲), 24-mer/36-N^2-IbG-mer (▼), and 24-mer/36-N^2-NaphG-mer (◆). All polymerization reactions were quenched with 0.3 M EDTA at various time intervals. The data were fit to the burst equation $y = A(1 - e^{-kpt}) + k_{ss}t$, as described under "Experimental Procedures" (without normalization of k_{ss} for enzyme concentration in the equation). Pre-steady-state rates (k_p) for the burst phase are indicated in the figure. The following rates were estimated: G-mer, $k_p = 3.6 \pm 0.5\ s^{-1}$, $k_{ss} = 0.36 \pm 0.02\ s^{-1}$; N^2-EtG-mer, $k_p = 2.6 \pm 5\ s^{-1}$, $k_{ss} = 0.11 \pm 0.01\ s^{-1}$; N^2-IbG-mer, $k_p = 0.80 \pm 0.34\ s^{-1}$, $k_{ss} = 0.063 \pm 0.002\ s^{-1}$, N^2-NaphG-mer, $k_p = 0.53 \pm 0.21\ s^{-1}$, $k_{ss} = 0.05 \pm 0.004\ s^{-1}$.

The burst of dCTP incorporation opposite N^2-EtG showed a 28% decreased rate with a small (20%) decrease of burst amplitude compared with G, suggestive of the presence of an inactive complex during polymerization opposite some adducts as in case of pol T7$^-$ and HIV-1 RT opposite 8-oxoG, O^6-MeG, N^2-MeG, and other adducts (17, 33, 47, 48) and pol η opposite N^2-EtG (18). The burst rates opposite N^2-IbG and N^2-NaphG were further decreased (5- and 7-fold, respectively) with further decreases (62 and 78%, respectively) of burst amplitude, compared with G. The burst rate opposite N^2-AnthG was decreased greatly to $0.16 \pm 0.04\ s^{-1}$ (if indeed, this is even a valid burst), which is about 23-fold slower than G but with similar amplitude as unmodified G (Fig. 4*C*). The k_{ss} rate in the second phase (steady-state) decreased as a function of bulk at the N2 atom of guanine. The k_{ss} rate ($0.35\ s^{-1}$) opposite unmodified G was similar as the k_{cat} value ($0.23\ s^{-1}$) in independent steady-state kinetic analysis and gradually decreased to 0.11, 0.06, 0.05, and $0.01\ s^{-1}$ opposite N^2-EtG, N^2-IbG, N^2-NaphG, and N^2-AnthG, respectively.

Phosphorothioate Analysis of dCTP Incorporation Opposite G and N^2-G Adducts by Pol ι—In considering whether the chemistry step (phosphodiester bond formation) might be rate-limiting, we compared the rates of incorporation of dCTP and S_p-dCTPαS opposite G, N^2-EtG, and N^2-AnthG. The pre-steady-state burst rates of incorporation opposite G and the N^2-G adducts were determined in a rapid quench instrument using dCTP and S_p-dCTPαS. S_p-dCTPαS was used, because it is a stereoselective dCTPαS substrate for DNA polymerases, including pol ι, and more relevant in thio effect analysis. Incorporation of R_p-dCTPαS opposite G showed a loss of the burst phase and markedly lower rate of incorporation (linear rate = $0.023\ s^{-1}$) compared with S_p-dCTPαS ($k_p = 2.2\ s^{-1}$) (*i.e.* ~100-fold slower; results not shown). If the rate of phosphodiester bond formation is rate-limiting, the incorporation rate of dCTPαS could be expected to be reduced compared with dCTP (49). Incorporation of S_p-dCTPαS opposite G yielded no significant decrease in the burst rate compared with dCTP (Fig. 4*A*). In contrast, incorporation of S_p-dCTPαS opposite N^2-EtG and N^2-AnthG yielded one linear phase (linear polymerization rates of $0.096\ s^{-1}$ and $0.016\ s^{-1}$, respectively) with no burst. Thus, the thio effects (ratio of the polymerization rate with dCTP to that with S_p-dCTPαS) were calculated to be ~27 and 11 with N^2-EtG and N^2-AnthG, respectively (Fig. 4, *B* and *C*), indicating that even a small ethyl group at the guanine N2 atom may cause the chemistry step to be rate-limiting in the polymerization cycle.

Active Site Titration and Estimation of Productive DNA Binding for Pol ι, K_d^{DNA}—The presence of a distinct pre-steady-state burst phase, indicating much faster catalysis than the equilibration of pol ι and DNA, enabled us to measure the active pol ι concentration and the equilibrium constant (K_d^{DNA}) for the pol ι-DNA complex by an enzyme active site titration with DNA substrate (41, 42). The pol ι·24/36-mer complex present in the preincubated *E*·DNA mixture was quantitated by quenching with EDTA after 0.5 s, which allowed adequate time to reach the maximal first turnover amplitude. The concentrations of products (measured in triplicate) were plotted against the DNA concentration and fit to a quadratic equation, yielding values for K_d^{DNA} of 61 ± 3 nM and an active pol ι concentration of 17 ± 1 nM, 13% of the UV (A_{280})-estimated protein concentration (Fig. 5). This result indicates that pol ι binds unmodified DNA with much lower affinity than other Y-family DNA polymerases ($K_d^{DNA} \cong 10$ nM), such as Dpo4 (50) and human pol η (18). The preparation of pol ι was ~13% active, which might represent the active fraction of G:C plus Hoogsteen base pairs having adequate hydrogen bonding (two bonds?) under these experimental conditions (pH 7.5) (and also might be attributable to another binding ability with blunt duplex DNA ends shown by pol ι (25, 26)). The concentration of pol ι was corrected for the amount of active enzyme in all other experiments.

Determination of K_d^{dCTP} for dCTP Incorporation by Pol ι—Analysis of the change of the pre-steady-state burst rate as a function of increasing

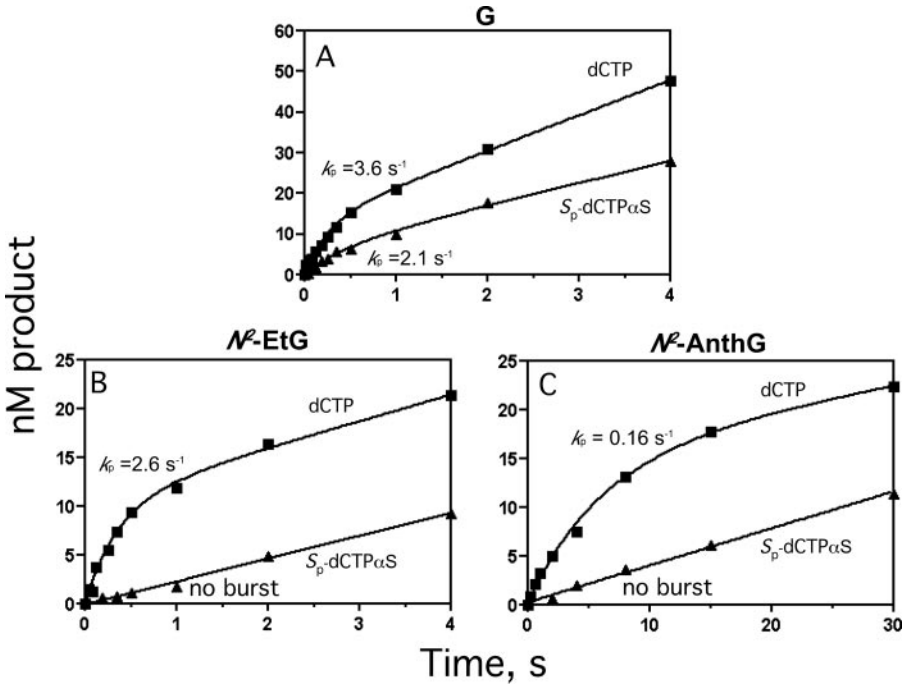

FIGURE 4. **Phosphorothioate analysis of pre-steady-state kinetics of nucleotide incorporation by human pol ι.** Pol ι (24 nM) was incubated with 100 nM 24-mer/36-mer primer-template complex in the rapid quench-flow instrument and mixed with 1 mM dCTP (■) or S_p-dCTPαS (●) to initiate reactions for the 24-mer/36-G-mer (*A*), 24-mer/36-N^2-EtG-mer (*B*), and 24-mer/36-N^2-AnthG-mer (*C*). The pre-steady-state rates were determined from the burst equation and are indicated in the figure. The *solid lines* represent the best fits to the burst equation or a linear equation (*B*; *C* with S_p-dCTPαS). The following rates were estimated. *A*, dCTP, $k_p = 3.6 \pm 0.5\ s^{-1}$; S_p-dCTPαS, $k_p = 2.1 \pm 0.6\ s^{-1}$. *B*, dCTP, $k_p = 2.6 \pm 5\ s^{-1}$; S_p-dCTPαS, $k = 0.096 \pm 0.004\ s^{-1}$. *C*, dCTP, $k_p = 0.16 \pm 0.04\ s^{-1}$; S_p-dCTPαS, $k = 0.015 \pm 0.001\ s^{-1}$.

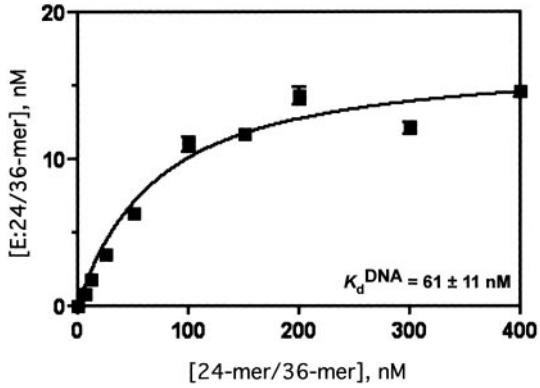

FIGURE 5. **Determination of K_d^{DNA} of human pol ι by active site titration.** Pol ι was incubated with increasing 24-mer/36-G-mer concentrations (■, 6–400 nM) and mixed with 1 mM dCTP to initiate the reaction. Reactions were quenched with EDTA after 0.5 s. A plot of burst amplitudes *versus* total DNA concentration was fit to a quadratic equation, as described under "Experimental Procedures," yielding an active site concentration of 17 ± 1 nM and $K_d^{DNA} = 61 \pm 11$ nM.

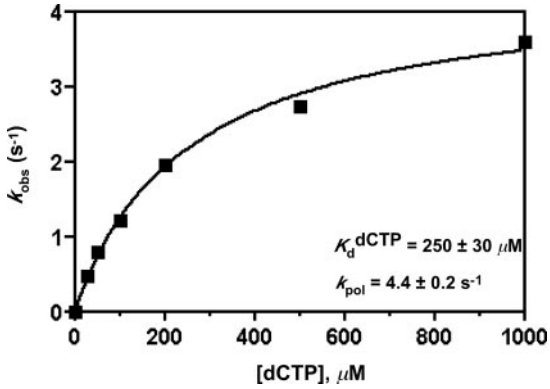

FIGURE 6. **Determination of K_d^{dCTP} with human pol ι by analysis of dCTP dependence of the pre-steady-state burst rates.** Pol ι (24 nM) was incubated with 100 nM 24-mer/36-mer primer-template complex in the rapid quench-flow instrument and mixed with increasing dCTP concentrations (■, 25–1000 μM) to initiate the reaction. Reactions were quenched with EDTA. A plot of burst rates (k_{obs}) *versus* [dCTP] was fit to a hyperbolic equation, as described under "Experimental Procedures," yielding k_{pol} (maximal rate of nucleotide incorporation) = 4.4 ± 0.2 s^{-1} and $K_d^{dCTP} = 250 \pm 30\ \mu M$.

dNTP concentration yields K_d^{dNTP}, a measure of the binding affinity of the dNTP to the *E*·DNA binary complex to form a ternary complex poised for catalysis (41, 42). The observed burst rates (k_{obs}) determined in the pre-steady-state reaction were plotted as a function of dNTP and fit to a hyperbolic equation, yielding a k_{pol} (maximal rate of nucleotide incorporation) of 4.4 ± 0.2 s^{-1} and a K_d^{dCTP} of 250 ± 30 μM with the unmodified DNA substrate (Fig. 6), indicating that pol ι binds loosely with the correct dCTP compared with other replicative DNA polymerases (K_d^{dCTP} ~1 μM) (*e.g.* pol T7$^-$ and HIV-1 RT) (32, 51).

DNA Dissociation Rates from Pol ι, k_{off}—The dissociation rates of *E*·DNA complexes were determined using DNA trapping experiments (Table 4). The preincubated E·DNA complex (unlabeled target DNA, 24-mer/36-mer with G or N^2-AnthG) was mixed with ^{32}P-labeled 24-mer/36-G-mer for varying time intervals (0.08–4 s). Polymerization was then initiated by the addition of dCTP-Mg^{2+} and continued for a constant time of 0.5 s (any polymerase dissociated from *E*·DNA would elongate the labeled trap DNA and not the unlabeled primer) (52). In this approach, the measurement does not rely on the incorporation rate opposite adducted DNA substrates but instead on unmodified DNA substrates (33). We compared N^2-AnthG-containing DNA with unmodified DNA on the DNA dissociation rate. Dissociation of unmodified DNA from pol ι occurred at rates of 1.5 ± 0.2 s^{-1} (Table 4). The dissociation rate (k_{off}) of N^2-AnthG-adducted DNA from pol ι decreased about 2-fold, compared with unmodified DNA, indicating that pol ι might dissociate from N^2-AnthG-adducted DNA somewhat more slowly than unmodified DNA.

Comparison of Primer Extension in the Presence of All Four dNTPs and Steady-state Kinetic Parameters of One-base Incorporation Opposite N^2-EtG and N^2,N^2-diMeG by Human Pol η and ι—Bypass abilities were compared opposite N^2-EtG and N^2,N^2-diMeG with human pol η and pol ι using primer extension and steady-state kinetic analysis. Processive polymerization opposite N^2-EtG and N^2,N^2-diMeG was analyzed in "running start" assays using 24-mer/36-mer duplexes containing N^2-EtG and N^2,N^2-diMeG (Fig. 1) at position 25 of the template (Fig. 7). Pol η readily extended the 24-mer primer annealed to the N^2-EtG template (in propor-

tion to the amount of enzyme) and yielded largely 35- and 36-mer products but was severely blocked opposite N^2,N^2-diMeG, with only a trace of extended products. However, pol ι showed similar bypass ability opposite N^2-EtG and N^2,N^2-diMeG, although having less subsequent extension ability beyond N^2,N^2-diMeG than N^2-EtG. This result was consistent with the steady-state kinetic analysis of one-base incorporation (Table 5). Whereas pol η showed a marked (190-fold) decrease of k_{cat}/K_m in dCTP incorporation opposite N^2,N^2-diMeG compared with N^2-EtG, pol ι showed no significant decrease of k_{cat}/K_m in dCTP incorporation opposite both adducts. Interestingly, pol ι demonstrated preferential dTTP misincorporation opposite N^2,N^2-diMeG ($f = 4.8$) instead of dCTP, compared with N^2-EtG ($f = 0.35$), indicating that the shape of the chemical moiety at guanine N2 can also affect the preference of dNTP opposite N^2-G adducts by pol ι, and the strong blockage beyond N^2,N^2-diMeG may be due to blocked extension from a mispair with T.

DISCUSSION

In this study, we systematically examined the effect of size at the minor groove side guanine (G) N2 atom of a DNA substrate on the bypass ability and the fidelity by one of the human TLS DNA polymerases, pol ι. Increasing bulk or, alternatively, hydrophobicity (see below) at G N2 noticeably attenuated the bypass ability in both steps, incorporation opposite lesion, and the subsequent extension by pol ι, with a high misincorporation of T. Bulk equal to or greater in size than the (methyl)naphthyl group produced a strong blockage of bypass opposite those lesions. The high thio effects opposite N^2-EtG and N^2-AnthG (but not opposite G) (Fig. 4) suggest that with pol ι the step of phosphodiester bond formation may be affected by even a small ethyl group at the G N2 atom. Several intrinsic kinetic properties of pol ι, including the low synthesis rate (k_{pol}), the high error frequency (f), and low affinities (K_d) for DNA and dCTP, may help explain the limited ability of pol ι for TLS opposite N^2-G adducts. These kinetic studies indicate that the role of pol ι may be greatly limited in the TLS across bulky N^2-G adducts, although it has been speculated that pol ι could bypass minor groove adducts efficiently by positioning G N2-bulk to the spacious major groove side of DNA to form a Hoogsteen base pair.

Even an intermediate sized adduct at the guanine N2 atom exerted a detrimental effect on both catalytic efficiency and fidelity of polymerization by pol ι. An isobutyl group interfered with the polymerization opposite a lesion, and a benzyl group interfered with the polymerization in both steps of the incorporation opposite a lesion and the subsequent extension (Figs. 2, 3, and 8 and Tables 2 and 3). A plot of k_{cat}/K_m *versus* the molecular volume of the substituent at the guanine N2 atom (Fig. 8*A*) indicates that the catalytic efficiency of pol ι is quite vulnerable to even small bulk (*e.g.* a methyl group) during incorporation opposite lesions and that this detrimental effect is largely dependent on the size of the N^2-G adduct. A decrease in k_{cat}/K_m for dCTP incorporation with pol ι was observed opposite even N^2-MeG (9-fold) and N^2-IbG (12-fold), in contrast to pol η, although the maximal extent of decrease in k_{cat}/K_m by bulk with pol ι (62-fold) was 6-fold less than pol η (320-fold) (18). Interestingly, the k_{cat}/K_m for next-base extension from matched G:C template-primer termini was not proportional to the volume of the bulk at guanine N2 (Fig. 8*B*). The small bulk of Me and Et groups rather gradually improved k_{cat}/K_m (up to 9-fold) compared with a hydrogen. The bulk of the (methyl)naphthyl group most severely interfered with the next-base extension, which is in good agreement with the strong blockage after one-base incorporation at N^2-NaphG (Fig. 2). Therefore, bulk size may not fully explain this phenomenon, and several other factors, such as the chemical properties, shape, and positioning, may affect next-base extension by physical and/or functional assistance or interference with the free 3′-OH group of incorporated nucleotide at 3′ primer termini and critical amino acid residues in the active site of pol ι.

Thus far in the discussion and in previous work with viral polymerases and pol η (17, 18), the effects of the changes seen with this series have been interpreted in the context of bulk of the N^2-guanyl adduct (*i.e.* steric considerations). However, the hydrophobicity of the adduct and the entire base increase along with the steric bulk in this series. We estimated the hydrophobicity of each of the N^2-substituted guanine bases, using four different software programs, ChemDraw Ultra (CambridgeSoft, Cambridge, MA), SciFinder/ACD (American Chemical Society, Washington, D. C.), MolInspiration (available on the World Wide Web at www.molinspiration.com), and LogP (available on the

TABLE 4
Rates of DNA dissociation from human pol ι (k_{off})

Dissociated complex	Rate
	s^{-1}
E·24/36-G	1.5 ± 0.2
E·24/36-N^2-AnthG	0.8 ± 0.2

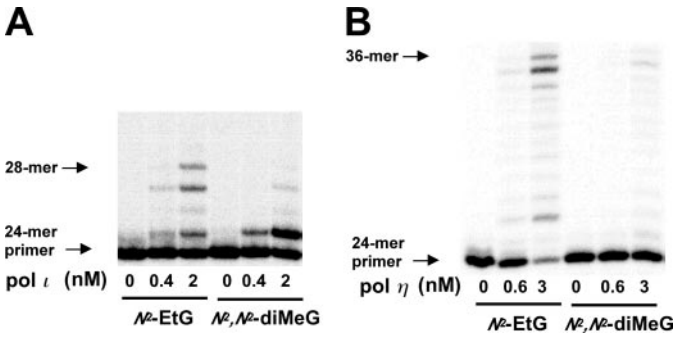

FIGURE 7. **Extension of ^{32}P-labeled 24-mer primer across N^2-EtG and N^2,N^2-diMeG, by human pol ι and η in the presence of all four dNTPs.** ^{32}P-Labeled 24-mer primer was annealed with 36-mer templates (Table 1) containing an N^2-EtG and N^2,N^2-diMeG placed at the 25th position from the 3′-end. ^{32}P-Labeled 24-mer primer was extended in the presence of all four dNTPs for 15 min with increasing amounts of pol ι (0–2 nM) (*A*) and pol η (0–3 nM) (*B*) and a constant concentration of DNA substrate (100 nM primer-template) as indicated. The reaction products were analyzed by denaturing gel electrophoresis with subsequent phosphorimaging analysis.

TABLE 5
Comparison of steady-state kinetic parameters for one-base incorporation opposite N^2-EtG and N^2, N^2-diMeG by human pol η and ι

Polymerase	Template:dNTP	K_m	k_{cat}	k_{cat}/K_m	-Fold difference of k_{cat}/K_m, compared with N^2-EtG	f (misinsertion ratio)
		μM	s^{-1}	$mM^{-1}\,s^{-1}$		
Pol η	N^2-EtG:dCTP	3.1 ± 0.6	0.31 ± 0.015	97		1
	N^2' N^2-diMeG:dCTP	140 ± 50	0.07 ± 0.008	0.5	190-fold lower	1
	N^2-EtG:dTTP	57 ± 8	0.135 ± 0.005	2.4		0.025
	N^2,N^2-diMeG:dTTP	300 ± 70	0.07 ± 0.007	0.25	10-fold lower	0.5
Pol ι	N^2-EtG:dCTP	190 ± 28	0.12 ± 0.01	0.63		1
	N^2,N^2-diMeG:dCTP	210 ± 31	0.11 ± 0.01	0.52	~1-fold	1
	N^2-EtG:dTTP	1100 ± 100	0.38 ± 0.01	0.35		0.56
	N^2,N^2-diMeG:dTTP	110 ± 15	0.28 ± 0.01	2.5	7-foldhigher	4.8

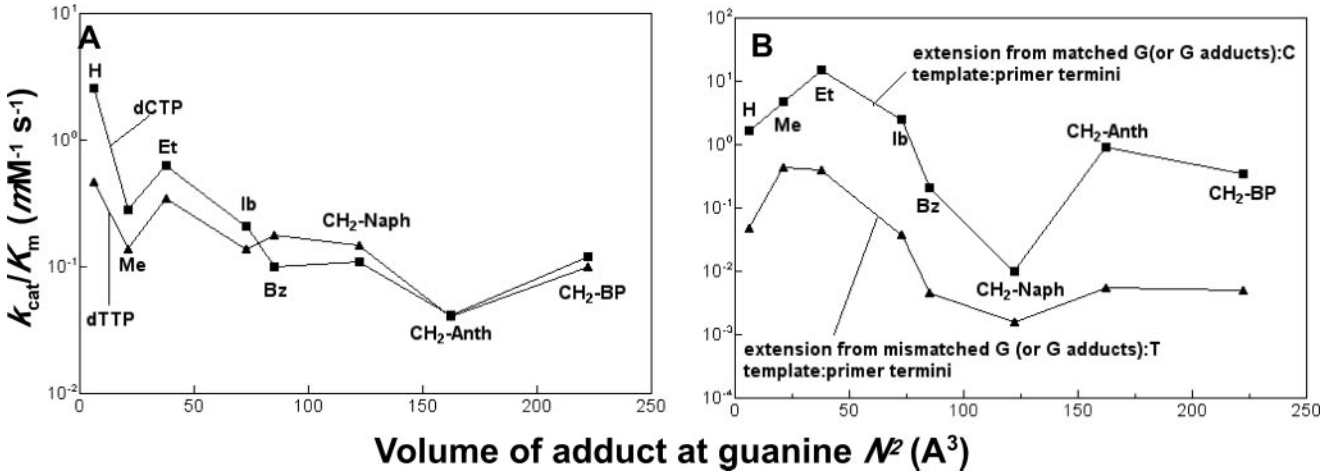

FIGURE 8. **Effect of the volume of adducts at the guanine N2 atom on catalytic efficiency (k_{cat}/K_m) for dCTP incorporation opposite N^2-G adducts by human pol ι.** *A*, the molecular volumes (Å^3) of adducts at the guanine N2 atom were calculated using the program Chem3D (version 7.0) based on the Connolly surface algorithm (53) and plotted against $\log_{10}(k_{cat}/K_m)$ values (Table 2) for dCTP (■) and dATP (▲) incorporation for various N^2-G adducts by pol ι. *B*, molecular volumes (Å^3) of adducts at the guanine N2 atom plotted against $\log_{10}(k_{cat}/K_m)$ values (Table 3) for next-base extension by dGTP from matched G (or N^2-G adducts):C template-primer termini (■) or mismatched G (or N^2-G adducts):T template-primer termini (▲) by pol ι.

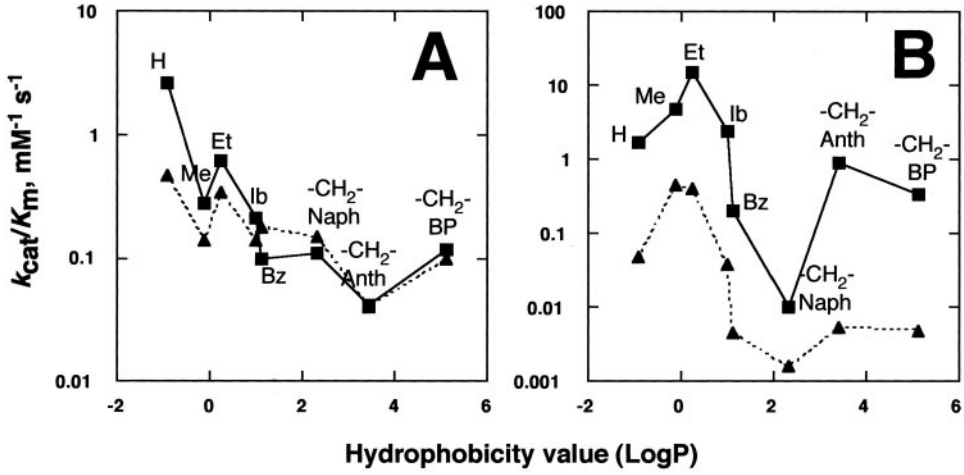

FIGURE 9. **Effect of the hydrophobicity of adducts at the guanine N2 atom on catalytic efficiency (k_{cat}/K_m) for dCTP incorporation opposite N^2-G adducts by human pol ι.** *A*, the hydrophobicity of modified guanines was estimated using log P (octanol/H_2O partition ratio) values calculated from the program MolInspiration (available on the World Wide Web at www.molinspiration.com/cgi-bin/properties) and plotted against $\log_{10}(k_{cat}/K_m)$ values (Table 2) for dCTP (■) and dATP (▲) incorporation for various N^2-G adducts by pol ι. *B*, log *p* values plotted against $\log_{10}(k_{cat}/K_m)$ values (Table 3) for next-base extension by dGTP from matched G (or N^2-G adducts):C template-primer termini (■) or mismatched G (or N^2-G adducts):T template-primer termini (▲) by pol ι.

World Wide Web at www.logp.com), all of which produced similar patterns. The plots with MolInspiration are shown in Fig. 9 and resemble those in Fig. 8 for bulk volume. Hydrophobicity, as judged by the estimated octanol-H_2O partition ratio, is clearly directly related to the volume of the alkyl and alkaryl groups in this series, and a clear distinction cannot be made between the two. In principle, a larger series of substituted bases might provide a separation of the two effects, although the problem of introducing other interactive factors (*e.g.* charge pairing and hydrogen bonding) would be an issue.

Patterns of changes of k_{cat}/K_m in next-base extension from mismatched G:T template-primer termini are similar to the matched G:C pair. Primer extension across lesions was markedly blocked by bulk equal to or greater than that of the N^2-NaphG group (Fig. 2), whereas the pre-steady-state burst rate of cytosine incorporation opposite the lesion was markedly reduced by size equal to or greater than that of N^2-IbG (Fig. 3). This discrepancy might be attributed to the good ability for subsequent extension beyond N^2-IbG and N^2-BzG and poor ability beyond N^2-NaphG (Fig. 8*B*). Primer extension in the presence of all four dNTPs involves the complete bypass process, including incorporation opposite a lesion and further extension, and therefore it can be affected by the type of incorporated dNTP. Bulk (or possibly hydrophobicity; see below) at G N2 can increase the frequency of misincorporation of T by pol ι (Table 2). Pol ι has an intrinsically high frequency of dTTP misincorporation opposite G ($f \sim 0.2$), which may be due to the Hoogsteen base-pairing mode in polymerization. Size at G N2 further increased the error rates of T incorporation ($f = 0.5$–1.8), with the highest opposite N^2-BzG. High error rates ($f \geq 1$) of T incorporation opposite N^2-BzG and bulkier adducts may contribute to the marked stalling, even after successful one-base incorporation opposite those lesions (Fig. 2).

The bypass ability of pol ι is greater than that of replicative DNA polymerases such as HIV-1 RT, T7$^-$, and pol δ but is less than that of pol η, another Y-family DNA polymerase. HIV-1 RT and T7$^-$ can partially bypass N^2-MeG only but are completely blocked opposite larger adducts. Pol δ bypasses up to N^2-EtG but is blocked opposite larger lesions, and pol η can bypass a lesion as large as N^2-NaphG effectively (17, 18). Our results indicate that pol ι can effectively bypass adducts up to N^2-EtG and partially bypass intermediate sized adducts, such as N^2-IbG and N^2-BzG, but is severely blocked at N^2-NaphG and larger adducts. Pol ι has an intrinsic low

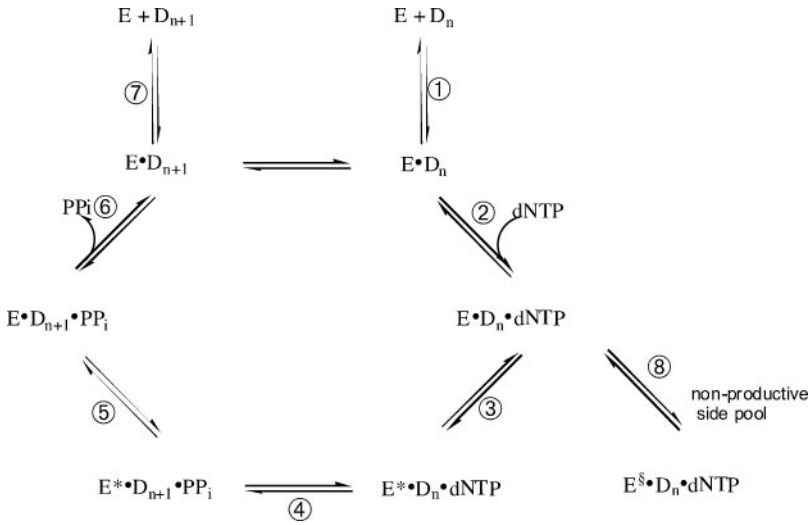

FIGURE 10. **General kinetic mechanism for DNA polymerization.** Individual steps are numbered. *E*, pol η; D_n, DNA substrate; *E**, conformationally altered polymerase; $E^§$, nonproductive conformation of polymerase, D_{n+1}, DNA extended by 1 base; *PPi*, pyrophosphate.

maximal polymerization rate (k_{pol}) of dCTP incorporation, low binding affinity (K_d^{DNA}) for DNA, and low binding affinity (K_d^{dCTP}) for dCTP. The k_{pol} rate (4.4 s^{-1}) of pol ι is 9-fold less than that of pol η (40 s^{-1}). The K_d^{DNA} determined by active site titration reflects productive binding of DNA; pol ι binds less tightly (5-fold) with DNA than pol η (61 *versus* 13 nM) (the binding affinity for DNA with template A at the primer-template junction with pol ι is similarly low (K_d^{DNA} = 44 nM) (54)). The K_d^{dCTP} for pol ι is 250 μM, indicating somewhat less affinity than in the case of pol η (140 μM). These properties and also the high T insertion error-induced stalling may contribute to a low processivity by pol ι in full-length extension (Fig. 2).

Which step of the catalytic cycle (Fig. 10) of pol ι can be affected by bulk? A low thio effect for the reaction opposite G suggests that the chemistry step of phosphodiester bond formation (Fig. 10, *step 4*) is not rate-limiting in correct dCTP incorporation opposite G. However, large thio effects opposite N^2-EtG and N^2-AnthG (>10) suggest that the chemistry step, the phosphodiester bond formation step (step 4), may be affected by even the bulk of a small ethyl group and can be rate-limiting.[3] These results are contrasted with our previous report of thio effects on human pol η (18), which suggests that step 3, preceding chemistry, might be largely affected by the bulk of N^2-AnthG. The thio effect on Dpo4 was 1.4 for correct base incorporation but was 5.9 for incorrect base incorporations, suggesting that the conformation step (step 3) might be rate-limiting for correct base incorporation, but the chemistry step (step 4) might be rate-limiting for incorrect base incorporation with Dpo4 (50). DNA containing N^2-AnthG dissociates only about 2-fold more slowly from pol ι than unmodified DNA. The estimated processivity of pol ι, calculated by k_{pol}/k_{off} (at 37 °C under these experimental conditions), is ~3 opposite template G and ~0.2 opposite N^2-AnthG, which is less than pol η (17 for G, 1.1 for N^2-AnthG) (18) and Dpo4 (16 for unmodified DNA) (50).

Pol ι may not always form Watson-Crick base pairs in the process of polymerization (26). Although N^2-EtG and N^2,N^2-diMeG have the same volume of bulk at guanine N2, N^2,N^2-diMeG has no hydrogen atom at guanine N2 position for hydrogen bonding with dCTP in a Watson-Crick G:C base-pairing mode, whereas N^2-EtG has one hydrogen atom remaining at that position. N^2,N^2-diMeG (no hydrogen atom at N2) markedly interfered with polymerization by pol η, but not by pol ι (Fig. 7, Table 5). One explanation of these results is that a hydrogen atom at guanine N2 is critical for efficient bypass opposite N^2-G adducts by pol η but not pol ι. The use of a Hoogsteen base-pairing mode by pol ι (but not pol η) during polymerization is consistent with this view but does not prove it. Interestingly, pol ι showed a much higher frequency of T misincorporation opposite N^2,N^2-diMeG than N^2-EtG, which suggests that the different shape of the dimethyl group in N^2,N^2-diMeG may induce the dTTP preference. The shape differences could be an issue, instead of the availability of a hydrogen bond (although the similarity of kinetic parameters for N^2-MeG and N^2-EtG adducts should be noted) (Figs. 8 and 9, Tables 2 and 3). Another point to be made is that efficient reactions can occur with two hydrogen bonds instead of three (*e.g.* A:T pairing), so the dramatic result (Fig. 7) probably has a more complex explanation.

How can the bulk at guanine N2 be positioned in the active site and affect the catalytic activity and fidelity by pol ι? The structure of a ternary complex of pol ι with template G:dCTP (26) shows that the N2 atom of guanine in the template is positioned at the major groove side of DNA in the active site with Hoogsteen base pairing. The pol ι active site favors Hoogsteen base pairing, wherein the template sugar is fixed in a cavity that reduces the C1′–C1′ distance across the nascent base pair from ~10.5 Å in other DNA polymerases to 8.6 Å in pol ι. Thus, it has been proposed that pol ι can locate the bulk at guanine N2 in the spacious major groove side and easily bypass N^2-adducted guanines that obstruct replication. Nevertheless, our data show that a small increase in the bulk (isobutyl group) can interfere with the polymerization by pol ι. The N2 atom of guanine is quite distant from the surrounding amino acids with about 5–12 Å open in some directions, and thus the available space at this position could be large enough for accommodating an isobutyl or benzyl group. An isobutyl or benzyl group at guanine N2 might be placed well in the spacious major groove side of DNA in the active site of pol ι. The possible contribution of hydrophobicity has been discussed (Fig. 9) as an issue in interpreting the results, although the phenomenon might seem inherently less likely to contribute than a steric effect. However, our kinetic data indicate that the bulk at guanine N2 can interfere somehow with phosphodiester bond formation in the kinetic cycle of pol ι, presumably by disturbing the coordination of three catalytic residues (Asp^{34}, Asp^{126}, and Glu^{127}) with two metal ions required for catalysis of nucleotidyl transfer. Therefore, the capability of pol ι to bypass bulky N^2-G adducts might be restricted by a kinetic factor, despite a favorable base-pairing mode with minor groove DNA adduct. A similar kinetic property of pol ι, which incorporates preferentially both C and T opposite G and N^2-G adducts, also suggests that Hoogsteen base pairing may take place between C (T) and N^2-G adducts during polymerization.

[3] Although some controversy exists regarding interpretation of the magnitude of sulfur elemental effects seen with dNTPαS, due to the varied transition states among different polymerases (49), and the interpretation of our results cannot be considered unambiguous, the existence of major differences in these values among polymerases and specific DNA adducts argues that they should not be ignored (30).

Multiple DNA polymerases may play a role in TLS across bulky N^2-G adducts in cells. Pol δ can bypass N^2-G adducts up to N^2-EtG effectively but not N^2-IbG (18). Therefore, the other TLS pols, such as pol η, might be required to replicate through the N^2-G adducts larger than N^2-EtG (18). Pol ι accumulates at replication foci with pol η, following DNA damage in human cells (55). Therefore, pol η and pol ι may cooperate in TLS across DNA adducts, such as N^2-G adducts. Considering the kinetic aspects, for the medium sized N^2-G adducts (up to N^2-NaphG), pol η (with higher efficiency) may dominate in bypass of N^2-G adducts, compared with pol ι. With ring-closed 1,N^2-G adducts, which cannot form Watson-Crick base pairs, pol ι might play a main role in bypass via Hoogsteen base-pairing. Only pol ι, and not pol η or κ, is able to incorporate nucleotides opposite the ring-closed adduct 8-hydroxy-1,N^2-propanoG (56). Our preliminary results with 1,N^2-ethenoG also suggest that both pol η and ι, but not pol κ, are able to replicate through the lesions with reduced efficiency. Pol κ also partially accumulates at replication foci after DNA damage such as UV and BPDE treatment (57, 58). Interestingly, BPDE treatment induced the relocalization of pol κ to nuclear foci but not pol η (59). Therefore, the sources and types of DNA damage may influence the recruitment of specific TLS pols to the stalled replication fork after DNA damage. The x-ray crystal structure of Rev1 also suggests a role for TLS across minor groove DNA adducts (60). Pol ζ is suggested to play a role as an extender in lesion bypass (7). Thus, analysis of the effect of bulk at guanine N2 on polymerization (insertion opposite lesion and the further extension) by pol κ, Rev1, pol ζ, and combinations of multiple polymerases is desired for understanding of the entire lesion bypass. When bypassing N^2-G adducts, pol ι may not complete the whole mutagenic bypass due to the high error of T misinsertion and low efficiency of next-base extension from T:G mismatch. Therefore, misinserted products produced by pol ι should be further processed with other DNA polymerases with switching if it is an error fixation or a correction. Mismatch extenders such as pol κ and ζ may extend the misinserted products and thus fix the error, or polymerases, such as pol δ and ε, may proofread and correct the error (thus causing other TLS pols to process it again).

In conclusion, our results indicate that human pol ι, one of the TLS DNA polymerases, may play a limited and error-prone role in TLS across the N^2-G adducts (possibly medium sized adducts up to N^2-BzG) due to the low polymerization rates and high error rates.

Acknowledgments—We thank K. C. Angel for technical assistance, E. M. Isin for calculating the hydrophobicity parameters, and K. Trisler for help in preparation of the manuscript.

REFERENCES

1. Kornberg, A., and Baker, T. A. (1992) *DNA Replication*, 2nd Ed., W. H. Freeman, New York
2. Searle, C. E. (1984) *Chemical Carcinogens*, Vols. 1 and 2, American Chemical Society, Washington, D. C.
3. Friedberg, E., Walker, G. C., Siede, W., Wood, R. D., Schultz, R. A., and Ellenberger, T. (2006) *DNA Repair and Mutagenesis*, 2nd Ed., American Society for Microbiolgy, Washington, D. C.
4. Friedberg, E. C., Wagner, R., and Radman, M. (2002) *Science* **296,** 1627–1630
5. Goodman, M. F. (2002) *Annu. Rev. Biochem.* **71,** 17–50
6. Ohmori, H., Friedberg, E. C., Fuchs, R. P. P., Goodman, M. F., Hanaoka, F., Hinkle, D., Kunkel, T. A., Lawrence, C. W., Livneh, Z., Nohmi, T., Prakash, L., Prakash, S., Todo, T., Walker, G. C., Wang, Z. G., and Woodgate, R. (2001) *Mol. Cell* **8,** 7–8
7. Prakash, S., Johnson, R. E., and Prakash, L. (2005) *Annu. Rev. Biochem.* **74,** 317–353
8. Yasui, M., Matsui, S., Ihara, M., Laxmi, Y. R., Shibutani, S., and Matsuda, T. (2001) *Nucleic Acids Res.* **29,** 1994–2001
9. Terashima, I., Matsuda, T., Fang, T.-W., Suzuki, N., Kobayashi, J., Kohda, K., and Shibutani, S. (2001) *Biochemistry* **40,** 4106–4114
10. Forgacs, E., Latham, G., Beard, W. A., Prasad, R., Bebenek, K., Kunkel, T. A., Wilson, S. H., and Lloyd, R. S. (1997) *J. Biol. Chem.* **272,** 8525–8530
11. Turesky, R. J., Rossi, S. C., Welti, D. H., Lay, J. O., Jr., and Kadlubar, F. F. (1992) *Chem. Res. Toxicol.* **5,** 479–490
12. Kim, D., and Guengerich, F. P. (2005) *Annu. Rev. Pharmacol. Toxicol.* **45,** 27–49
13. Meehan, T., and Straub, K. (1979) *Nature* **277,** 410–412
14. Cheng, S. C., Hilton, B. D., Roman, J. M., and Dipple, A. (1989) *Chem. Res. Toxicol.* **2,** 334–340
15. Fang, J. L., and Vaca, C. E. (1997) *Carcinogenesis* **18,** 627–632
16. Matsuda, T., Terashima, I., Matsumoto, Y., Yabushita, H., Matsui, S., and Shibutani, S. (1999) *Biochemistry* **38,** 929–935
17. Choi, J-Y., and Guengerich, F. P. (2004) *J. Biol. Chem.* **279,** 19217–19229
18. Choi, J-Y., and Guengerich, F. P. (2005) *J. Mol. Biol.* **352,** 72–90
19. Tissier, A., McDonald, J. P., Frank, E. G., and Woodgate, R. (2000) *Genes Dev.* **14,** 1642–1650
20. Johnson, R. E., Washington, M. T., Haracska, L., Prakash, S., and Prakash, L. (2000) *Nature* **406,** 1015–1019
21. Zhang, Y., Yuan, F., Wu, X., and Wang, Z. (2000) *Mol. Cell. Biol.* **20,** 7099–7108
22. Tissier, A., Frank, E. G., McDonald, J. P., Iwai, S., Hanaoka, F., and Woodgate, R. (2000) *EMBO J.* **19,** 5259–5266
23. Frank, E. G., Sayer, J. M., Kroth, H., Ohashi, E., Ohmori, H., Jerina, D. M., and Woodgate, R. (2002) *Nucleic Acids Res.* **30,** 5284–5292
24. Washington, M. T., Minko, I. G., Johnson, R. E., Wolfle, W. T., Harris, T. M., Lloyd, R. S., Prakash, S., and Prakash, L. (2004) *Mol. Cell. Biol.* **24,** 5687–5693
25. Nair, D. T., Johnson, R. E., Prakash, S., Prakash, L., and Aggarwal, A. K. (2004) *Nature* **430,** 377–380
26. Nair, D. T., Johnson, R. E., Prakash, L., Prakash, S., and Aggarwal, A. K. (2005) *Structure* (*Camb.*) **13,** 1569–1577
27. Wang, M., Devereux, T. R., Vikis, H. G., McCulloch, S. D., Holliday, W., Anna, C., Wang, Y., Bebenek, K., Kunkel, T. A., Guan, K., and You, M. (2004) *Cancer Res.* **64,** 1924–1931
28. Albertella, M. R., Lau, A., and O'Connor, M. J. (2005) *DNA Repair* (*Amst.*) **4,** 583–593
29. Yang, J., Chen, Z., Liu, Y., Hickey, R. J., and Malkas, L. H. (2004) *Cancer Res.* **64,** 5597–5607
30. Guengerich, F. P. (2006) *Chem. Rev.* **106,** 420–452
31. Furge, L. L., and Guengerich, F. P. (1997) *Biochemistry* **36,** 6475–6487
32. Woodside, A. M., and Guengerich, F. P. (2002) *Biochemistry* **41,** 1027–1038
33. Woodside, A. M., and Guengerich, F. P. (2002) *Biochemistry* **41,** 1039–1050
34. Zang, H., Harris, T. M., and Guengerich, F. P. (2005) *Chem. Res. Toxicol.* **18,** 389–400
35. Zang, H., Harris, T. M., and Guengerich, F. P. (2005) *J. Biol. Chem.* **280,** 1165–1178
36. Einolf, H. J., Schnetz-Boutaud, N., and Guengerich, F. P. (1998) *Biochemistry* **37,** 13300–13312
37. Harris, C. M., Zhou, L., Strand, E. A., and Harris, T. M. (1991) *J. Am. Chem. Soc.* **113,** 4328–4329
38. Borer, P. N. (1975) in *Handbook of Biochemistry and Molecular Biology* (Fasman, G. D., ed) 3rd Ed., CRC Press, Cleveland, OH
39. Wray, W., Boulikas, T., Wray, V. P., and Hancock, R. (1981) *Anal. Biochem.* **118,** 197–203
40. Goodman, M. F., Creighton, S., Bloom, L. B., and Petruska, J. (1993) *Crit. Rev. Biochem. Mol. Biol.* **28,** 83–126
41. Patel, S. S., Wong, I., and Johnson, K. A. (1991) *Biochemistry* **30,** 511–525
42. Johnson, K. A. (1995) *Methods Enzymol.* **249,** 38–61
43. Wong, I., Patel, S. S., and Johnson, K. A. (1991) *Biochemistry* **30,** 526–537
44. Zinnen, S., Hsieh, J. C., and Modrich, P. (1994) *J. Biol. Chem.* **269,** 24195–24202
45. Suo, Z., and Johnson, K. A. (1997) *Biochemistry* **36,** 12459–12467
46. Mendelman, L. V., Petruska, J., and Goodman, M. F. (1990) *J. Biol. Chem.* **265,** 2338–2346
47. Furge, L. L., and Guengerich, F. P. (1999) *Biochemistry* **38,** 4818–4825
48. Suo, Z., Lippard, S. J., and Johnson, K. A. (1999) *Biochemistry* **38,** 715–726
49. Herschlag, D., Piccirilli, J. A., and Cech, T. R. (1991) *Biochemistry* **30,** 4844–4854
50. Fiala, K. A., and Suo, Z. (2004) *Biochemistry* **43,** 2116–2125
51. Furge, L. L., and Guengerich, F. P. (1998) *Biochemistry* **37,** 3567–3574
52. Hsieh, J.-C., Zinnen, S., and Modrich, P. (1993) *J. Biol. Chem.* **268,** 24607–24613
53. Connolly, M. L. (1993) *J. Mol. Graph.* **11,** 139–141
54. Washington, M. T., Johnson, R. E., Prakash, L., and Prakash, S. (2004) *Mol. Cell. Biol.* **24,** 936–943
55. Kannouche, P., Fernandez de Henestrosa, A. R., Coull, B., Vidal, A. E., Gray, C., Zicha, D., Woodgate, R., and Lehmann, A. R. (2002) *EMBO J.* **21,** 6246–6256
56. Wolfle, W. T., Johnson, R. E., Minko, I. G., Lloyd, R. S., Prakash, S., and Prakash, L. (2005) *Mol. Cell. Biol.* **25,** 8748–8754
57. Bergoglio, V., Bavoux, C., Verbiest, V., Hoffmann, J. S., and Cazaux, C. (2002) *J. Cell Sci.* **115,** 4413–4418
58. Ogi, T., Kannouche, P., and Lehmann, A. R. (2005) *J. Cell Sci.* **118,** 129–136
59. Bi, X., Slater, D. M., Ohmori, H., and Vaziri, C. (2005) *J. Biol. Chem.* **280,** 22343–22355
60. Nair, D. T., Johnson, R. E., Prakash, L., Prakash, S., and Aggarwal, A. K. (2005) *Science* **309,** 2219–2222

SUPPLEMENTAL DATA

J. Biol. Chem. 281, 000-000

Jeong-Yun Choi and F. Peter Guengerich

Kinetic Evidence for Inefficient and Error-prone Bypass across Bulky N^2-Guanine DNA Adducts by Human DNA Polymerase ι

FIG. S1. MALDI/TOF MS and capillary gel elctrophoresis analysis of N^2,N^2-dimethylG 36-mer.

FIG. S2. Analysis of purified human pol ι.

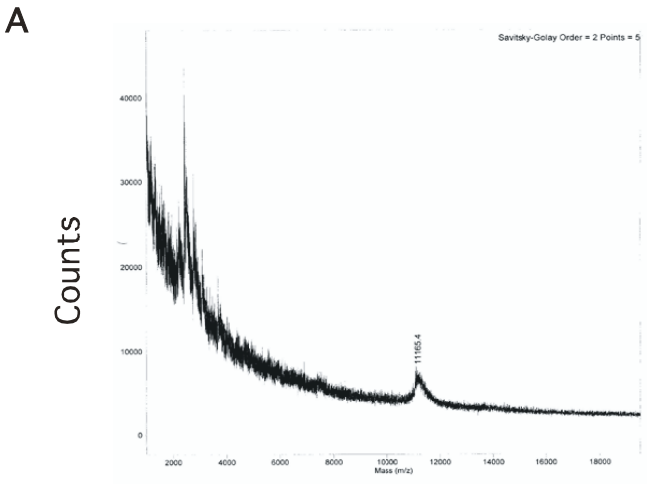

***m/z* calcd. for $[MH]^+$ 11166.4, found 11165.4**

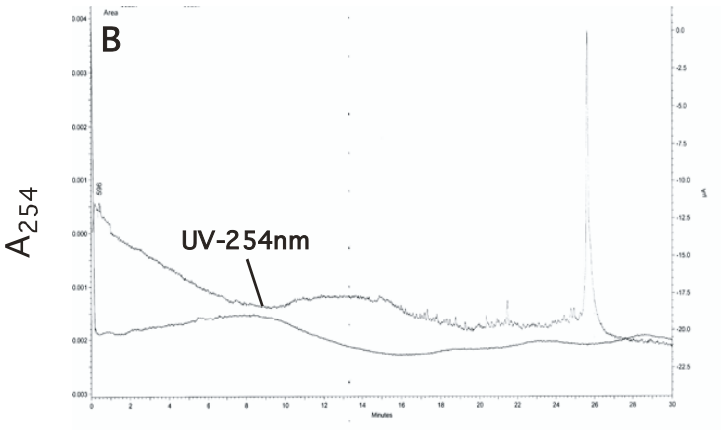

FIG. S1. MALDI/TOF MS and capillary gel electrophoresis analysis of N^2,N^2-dimethylG 36-mer.

A, The mass spectrum was obtained using a Voyager Elite DE instrument (Perseptive Biosystems). The system was operated in the linear positive ion mode using a matrix mixture of 0.25 M 3-hydroxypicolinic acid, 25 mM ammonium citrate, 0.1% CF_3CO_2H (v/v), and 30% CH_3CN (v/v). *B*, Capillary gel electrophoresis was performed on a Beckman P/ACE instrument using the manufacturer's ssDNA 100 gel capillary and Tris-borate-urea buffer. Samples were applied at 10 kV for 10 s and separated at 11 kV (30 °C). See references 17 and 18 for analytical data on other oligonucleotides.

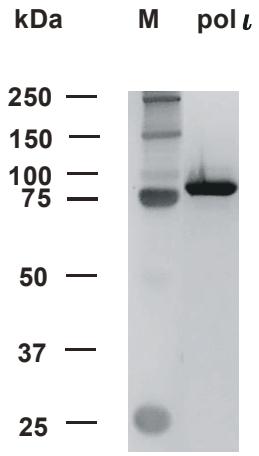

FIG. S2. Analysis of purified human pol ι. Purified recombinant DNA pol ι (100 ng) was analyzed by electrophoresis on a 10% (w/v) SDS-polyacrylamide gel and visualized by silver staining. Protein size markers (lane M) are shown on the left.

Kinetic Evidence for Inefficient and Error-prone Bypass across Bulky N^2-Guanine DNA Adducts by Human DNA Polymerase ι

Jeong-Yun Choi and F. Peter Guengerich

J. Biol. Chem. 2006, 281:12315-12324.
doi: 10.1074/jbc.M600112200 originally published online March 8, 2006